HHS Public Access

Author manuscript

Biosens Bioelectron X. Author manuscript; available in PMC 2024 August 01.

Published in final edited form as:

Biosens Bioelectron X. 2024 August ; 19: . doi:10.1016/j.biosx.2024.100490.

A digital microfluidic device integrated with electrochemical sensor and 3D matrix for detecting soluble PD-L1

Yuqian Zhang[a,b], **Jing Liu**[a,b], **Ting-Wen Lo**[a,b], **Yohan Kim**[c], **Fabrice Lucien**[c,d], **Haidong Dong**[c,d], **Yuguang Liu**[a,b,d,e,*]

[a]Department of Physiology & Biomedical Engineering, Mayo Clinic, Rochester, MN, 55905, USA

[b]Microbiomics Program, Center for Individualized Medicine, Mayo Clinic, Rochester, MN, 55905, USA

[c]Department of Urology, Mayo Clinic College of Medicine and Science, Rochester, MN, 55905, USA

[d]Department of Immunology, Mayo Clinic, Rochester, MN, 55905, USA

[e]Department of Surgery, Mayo Clinic, Rochester, MN, 55905, USA

Abstract

PD1/PD-L1 checkpoint inhibitors are at the forefront of cancer immunotherapies. However, the overall response rate remains only 10–30%. Even among initial responders, drug resistance often occurs, which can lead to prolonged use of a futile therapy in the race with the fatal disease. It would be ideal to closely monitor key indicators of patients' immune responsiveness, such as circulating PD-L1 levels. Traditional PD-L1 detection methods, such as ELISA, are limited in sensitivity and rely on core lab facilities, preventing their use for the regular monitoring. Electrochemical sensors exist as an attractive candidate for point-of-care tool, yet, streamlining multiple processes in a single platform remains a challenge. To overcome this challenge, this work integrated electrochemical sensor arrays into a digital microfluidic device to combine their distinct merits, so that soluble PD-L1 (sPD-L1) molecules can be rapidly detected in a programmed and automated manner. This new platform featured microscale electrochemical sensor arrays modified with electrically conductive 3D matrix, and can detect as low as 1 pg/mL sPD-L1 with high specificity. The sensors also have desired repeatability and can obtain reproducible results on

*Corresponding author. Department of Physiology & Biomedical Engineering, Mayo Clinic, Rochester, MN, 55905, USA. liu.yuguang@mayo.edu (Y. Liu).

CRediT authorship contribution statement

Yuqian Zhang: Writing – original draft, Visualization, Validation, Methodology, Investigation, Formal analysis, Data curation, Conceptualization. **Jing Liu:** Formal analysis, Investigation, Validation, Visualization, Writing – review & editing. **Ting-Wen Lo:** Validation, Visualization, Writing – review & editing. **Yohan Kim:** Methodology. **Fabrice Lucien:** Writing – review & editing, Methodology, Investigation. **Haidong Dong:** Writing – review & editing, Investigation. **Yuguang Liu:** Writing – review & editing, Supervision, Resources, Project administration, Investigation, Funding acquisition, Conceptualization.

Declaration of competing interest

The authors declare that they have no known competing financial interests or personal relationships that could have appeared to influence the work reported in this paper.

Appendix A. Supplementary data

Supplementary data to this article can be found online at https://doi.org/10.1016/j.biosx.2024.100490.

different days. To demonstrate the functionality of the device to process more complex biofluids, we used the device to detect sPD-L1 molecules secreted by human breast cancer cell line in culture media directly and observed 2X increase in signal compared with control experiment. This novel platform holds promise for the close monitoring of sPD-L1 level in human physiological fluids to evaluate the efficacy of PD-1/PD-L1 immunotherapy.

Keywords

Electrochemical detection of sPD-L1; Digital microfluidics; Cancer therapeutic monitoring; Immunotherapy monitoring

1. Introduction

Programmed death-ligand 1 (PD-L1) is a transmembrane immune checkpoint protein that can cause T cell exhaustion. The binding of PD-L1 on tumor cell membranes to its receptor, programmed cell death protein 1 (PD-1) on T cell membranes, can inhibit T cell activities such as proliferation and cytotoxicity, therefore promoting tumor growth (Gong et al., 2018; Han et al., 2020; Sunshine and Taube 2015). Blocking PD-1/PD-L1 interaction such as through immune checkpoint inhibitors has revolutionized cancer treatment as it leverages patient's immune system to fight cancer (Mahoney et al., 2015; Patsoukis et al.), including melanoma (Merelli et al., 2014), renal cell carcinoma (Massari et al., 2015) and lung cancer (Shien et al., 2016). Although PD-1/PD-L1 blockade therapies are at the forefront of cancer immunotherapies, their overall response rate remains only 10–30% and varies across tumor types and individuals.(Herbst et al., 2014). Even among initial responders, drug resistance often evolves, which is a key barrier to long-term remission. Prolonged use of a futile therapy on cancer patients can lead to the loss of time in the race with the fatal disease, as well as financial burden on patients, healthcare systems and economy(Nesline et al., 2020; Verma et al., 2018). Therefore, to ensure the ensure that patients are not exposed to an ineffective therapy while more fruitful alternatives are still an option, it is essential to regularly evaluate the responsiveness of PD-1/PD-L1 immune checkpoint blockade therapy.

Enzyme-linked immunosorbent assay (ELISA) is the most common method to measure the expression level of PD-L1 (Awad et al., 2016; Chen et al., 2011). It has been used to detect PD-L1 in dissociative forms, namely, soluble PD-L1 (sPD-L1), in samples such as serum and cell culture (Chen et al., 2011). Other methods of detecting PD-L1 with high sensitivity have also been reported, such as fluorescence (Hu et al., 2021; Li et al., 2020; Noguchi et al., 2020), chemiluminescence (Goto et al., 2019) and Surface Enhanced Raman Scattering (SERS) (Li et al., 2018; Ou et al., 2018). These methods typically rely on specialized bulky instrument in centralized laboratories and highly trained personnel, presenting a practical challenge to frequently using them for therapeutic response monitoring.

As an alternative, immunosensors have been gaining attention as they can be easily integrated with microfluidic technologies to create a point-of-care (POC) tool (Hu et al., 2023; Li and Lillehoj). In these sensors, antibodies conjugate with target analytes to produce specific changes in output signal. Among these, electrochemical-based immunosensors have been increasingly gaining popularity due to their high sensitivity, real-time measurement,

portability, and affordability. In fact, this technology has been developed and adapted in various formats to detect sPD-L1 molecules. For example, electrochemical sensors can detect sPD-L1 levels in whole blood, where sPD-L1 molecules were first captured on gold-coated magnetic nanoparticles as “dispersible electrodes” in regular tubes and achieved a detection limit of 15 aM within 15 min (Moazzam et al., 2021). Very recently, photonic methods have also been combined with electrochemical sensors to create photo-electrochemical sensing systems that can detect femtograms of sPD-L1 molecules (Li et al., 2023; Wang et al., 2023). While these new methods offer superior sensitivity in detection, each of the processes, including sample preparation, sample wash and target detection, are typically performed as distinct steps in regular tubes. New trends are moving toward POC testing by integrating microfluidics with electrochemical sensors. For example, electrochemical immunosensors were integrated with paper-based microfluidic devices to detect sPD-L1, where a highly conductive nanomaterial (amine-modified single-walled carbon nanotube) was functionalized on the electrode surface to enhance the electrode conductivity, which enabled a linear analysis of 10 pg/mL – 2.5 ng/mL (Xing et al. 2021, 2022). While these efforts represent significant progresses toward the rapid and sensitive detection of sPD-L1, these methodologies still require repeated manual processes including sPD-L1 extraction and sample wash, which are typically performed in regular tubes.

To enable the frequent assessment of PD-L1 levels, it would be ideal to miniaturize and streamline all these processes into a single platform while maintaining the sensitivity. Digital microfluidics (DMF) has emerged as an attractive option for POC testing due to its ability to handle droplets automatedly in a programmed manner (Zhang and Liu 2022a). This technology uses electrowetting-on-dielectric (EWOD) principle to automatedly manipulate microscale and nanoscale droplets on insulated electrodes under applied voltage (Nelson and Kim 2012), and the movement of the droplets can be accurately tracked in real-time based on machine vision (Li et al., 2021). To leverage the distinct merits of electrochemical immunosensors and DMF technology for POC testing, we previously integrated electrochemical impedance spectroscopy into a DMF device to rapidly quantify the abundance of human peripheral blood mononuclear cell (PBMC) (Zhang and Liu 2022b). Compared with PBMCs (5–30 μm), sPD-L1 molecules are in the range of nanoscale; therefore, detecting these molecules require biosensors with increased sensitivity.

To achieve this goal, in this work, we integrated a porous nanostructured 3D matrix on the sensing electrode to enhance the sensitivity of the electrochemical sensors. This is because, compared with a planar surface of an electrode, the nanostructure can provide a roughened surface and porous structure, which can accommodate increased number of target binding sites. The matrix is composed of a mixture of reduced graphene oxide (rGO), bovine serum albumin and glutaraldehyde, which features high electrical conductivity and meanwhile provides an antifouling coating to reduce non-specific binding (Sabaté del Río et al., 2019; Zupančič et al., 2021). As a proof-of-concept, we modified the surfaces of the electrochemical sensors with 3D matrix and integrated an array of electrochemical sensors into a DMF device. The device was able to detect as low as 1 pg/mL sPD-L1 in buffered sample with high specificity and demonstrated the feasibility to detect these molecules secreted by a human breast cancer cell line directly in culture medium.

2. Materials and methods

2.1. Materials

Bovine serum albumin (BSA), potassium chloride (KCl), potassium ferricyanide ($K_3[Fe(CN)_6]$), tetraethylene pentamine functionalized rGO (TEPA-rGO), 2-(N-morpholino)ethanesulfonic acid (MES), TWEEN® 20, glutaraldehyde (GA), Pluronic® F-68, Parylene C, and precipitating 3,3′,5,5′-Tetramethylbenzidine (TMB) were purchased from Sigma-Aldrich (St. Louis, MO, USA). 1-Ethyl-3-(3 dimethylaminopropyl)carbodiimide (EDC) and N-Hydroxysuccinimide (NHS) were purchased from Bruker (German). Phosphate buffered saline (PBS) was purchased from Corning (NY, USA). 10x Tris Buffered Saline (TBS) was purchased from Bio-Rad (USA). SuperBlock™ blocking buffer and poly-horseradish peroxidase (HRP) streptavidin were purchased from Thermo Fisher Scientific (Waltham, MA, USA). FluoroPel PFC1101V was purchased from Cytonix (Beltsville, MD, USA). Shipley S1811 photoresist was purchased from Rohm and Haas (Marlborough, MA, USA). Chrome (Cr)-coated glass slides was purchased from KLOE (Saint-Mathieu-de-Tréviers, France). Indium tin oxide (ITO) glass slide was purchased from Delta Technologies (Loveland, USA). Recombinant Human PD-L1/B7–H1 Fc Chimera Protein was obtained from Bio-techne (USA). Monoclonal mouse anti-human PD-L1 antibody was obtained from LS Bio (USA).

2.2. DMF device overview

Overall, the DMF device was controlled by a DropBot system (Scibots, Toronto, ON) for droplet handling (Fig. 1a). The device consisted of a bottom glass plate with arrays of actuation electrodes for droplet handling, and a top glass plate with an array of electrochemical electrodes for target detection (Fig. 1b). Each electrochemical electrode was drop-casted with a 3D matrix composed of rGO, BSA, and GA (Fig. 1c) to enhance target capture, electrical conductivity while minimize non-specific binding.

2.3. Fabrication of the bottom-plate

The DMF device was designed in AutoCAD (Autodesk, Mill Valley, CA, USA). The bottom layer of the device had 8 reservoir electrodes, 40 actuation electrodes (4 mm × 4 mm) and electrical contact pads, which was microfabricated using our established procedures (Liu et al., 2021; Liu and Papautsky 2019; Zhang and Liu 2022b). Briefly, electrodes were photolithographically patterned on chrome (Cr)-coated glass slides, and 5 μm Parylene C was deposited onto the substrate as an insulating layer (Specialty Coating Systems, Clear Lake, WI, USA). The substrate with spin-coated with FluoroPel PFC1101V as the hydrophobic layer, and incubated on a hot plate (160 °C, 30 min).

2.4. Fabrication of the top plate

The microsensor arrays in the top plate of the device was microfabricated on a 2”x3” ITO glass slide using photolithography and lift-off methodology (R_S = 8–12 Ω m/m, Delta Technologies Ltd., Stillwater, MN, USA). Briefly, the ITO substrate was spin-coated (3000 rpm, 30 s) with Shipley S1811 photoresist, and was photolithographically patterned. The glass slide was then spin-coated with a hydrophobic layer and treated with oxygen plasma

for 5 min (VLF-1000, Yield Engineering System, Inc., Fremont, CA, USA) to temporarily transform the hydrophobic layer into hydrophilic. Then, a second layer of S1811 photoresist was spin-coated on the substrate, and the space for electrochemical electrode array was patterned. After that, a layer of 10 nm Ti and 100 nm Au was deposited on the substrate via electron-beam physical vapor deposition (SQC-310, Inficon Bad Ragaz, Switzerland), and lift-off technology was then deployed. Finally, the substrate was immersed in acetone to remove the photoresist and incubated at 200 °C for 1 hour to restore hydrophobicity.

2.5. Surface functionalization of electrochemical electrode

The 3D matrix mixture solution was prepared using 5 mg/mL of BSA in PBS with 10 mg/mL of TEPA-rGO. The composite solution was then vortexed and sonicated for 5 h (Branson CPX1800H Ultrasonic Cleaner, Brookfield, CT, USA). The coating was then heat-denatured at 105 °C for 5 min. GA was then added to the clear nanomaterial supernatant solution in a 70:1 vol ratio the sensors (Sabaté del Río et al., 2019). The sensors were then incubated at 60 °C for 2 min, after which 40 <L of the nanomaterial solution was drop-casted over each sensor to form a conductive nanocomposite and was then washed with PBS.

After conjugating the matrix coating, the terminal carboxylic acid group was activated with MES buffer that contains 400 mM EDC and 200 mM NHS at room temperature for 30 min to form NHS ester. The working electrodes were subsequently incubated with antibodies (monoclonal anti-PD-Ll, 100 μg/mL) overnight at 4 °C. The surface of the electrodes was then incubated with SuperBlock™ blocking buffer for 2 h to minimize the non-specific absorption. The surface modification and the conjugation of antibody molecules on the electrode surface were verified using electrochemical characterization.

2.6. Characterization

The morphology of the 3D matrix structure was characterized with scanning electron microscopy (SEM, Noran EDC Hitachi). The surface modified working electrode was characterized with Raman spectroscopy (Witech Alpha 300R) to ensure the successful addition of each component. Briefly, a 785 nm laser was used, and Raman spectra were taken with 50 × /N.A. objective lens for laser focus. The integration time was set as 30 s to record the Raman spectra, and the data processing included baseline correction and smoothing. The thickness of the 3D matrix structure was estimated to be ~13 μm (P-7 Stylus Profiler, KLA).

2.7. Device assembly and operation

To complete the DMF device, the top and bottom substrates were assembled using an electrically conductive tape (127 μm) (3M, Ted Pella, Inc., Redding, CA, USA), so that the two plates were connected in parallel with a microscale space in-between for fluid handling. Each actuation electrode can support a 4 μL droplet. The device was operated in a Dropbot system (Sci-bot, Inc), and droplets were handled through MicroDrop software. Reagents were pipetted onto reservoir electrodes and dispensed as smaller droplets. The droplets were then moved across the electrochemical electrodes for incubation and sensing, and waste fluids were transferred to the waste reservoirs.

2.8. Preparation of sPD-L1 from cell culture media

Human MDA-MB-231 cells were transfected with a pcDNA3.1 vector containing full-length cDNA of human PD-L1. Transfection was done with Lipofectamine 3000 according to manufacturer's instructions. PD-L1 overexpressing cells were maintained in complete medium supplemented with G418 at a concentration 50 μg/mL. To generate soluble PD-L1, 231 cells were cultured in serum-free medium for 48 h. Culture medium was centrifuged at 2500×*g* to remove cell debris and aggregates. Supernatant was filtered using centrifugal filters (100 MWCO cut-off). PD-L1 knockout 231 cells were used as negative control. PD-L1 was knocked-out using CRISPR/Cas9 technology. The guide sequence (5'-ATTTACTGTCACGGTTCCCA-3') specific to human B7–H1 exon 3 (second coding exon), was designed using CRISPR DESIGN tool (http://crispr.mit.edu) and cloned into px458 plasmid coexpressing GFP (Addgene, #52961). Thirty-six hours after transfection, cells were sorted for GFP and sub-cloned using flow cytometry. Two weeks later, PD-L1 knockout cells were purified by flow cytometry using PD-L1 antibody (29E.2A3 clone).

2.9. Electrochemical based detection of PD-L1 protein

sPD-L1 sample (0.025%w/v Pluronic F-68) was serially diluted to 1 pg/mL – 1 ng/mL, and a droplet of each diluted sample was delivered to antibody-coated electrochemical sensor and incubated at room temperature for 1 hour (Fig. S1). Three droplets of wash buffer (0.1 M PBS, 0.025% w/v Pluronic F-68 and 0.05% w/v Tween 20) were sequentially passed over the sensing electrodes to wash away unbound molecules. A new droplet with biotinylated anti-PD-L1 detection antibodies (1 μg/mL, containing 0.025% w/v Pluronic F-68) was then moved to incubate with captured sPD-L1 for 30 min at room temperature. Sample wash was repeated for 3 times, and poly- HRP streptavidin (Thermo Fisher Scientific, Waltham, MA, USA) was incubated for 15 min, followed by another incubation of precipitating TMB for 5 min.

Electrochemical measurements were conducted using a CHI660E Potentiostat electrochemical workstation in a Picoamp Booster and Faraday Cage (CHI200B, CH Instruments, Inc., Austin, TX, USA). Cyclic voltammetry (CV) detection was conducted within a detection voltage from −0.8V to 0.4V under the scan rate of 100 mV/s in an electrolyte solution that contains 10 mM $K_3[Fe(CN)_6]/K_4[Fe(CN)_6]$ and a supporting electrolyte of 0.1 M KCl. Differential Pulse Voltammetry (DPV) was measured with the potential step, frequency and amplitude was set as 0.01V, 20 Hz and 50 mV. Electrochemical Impedance Spectroscopy (EIS) was carried out at frequency ranging from 0.1 HZ to 1 MHz under the initial voltage of 50 mV. The obtained electrochemical impedance spectra were plotted in the form of a Nyquist plot for further equivalent circuit fitting.

3. Results and discussion

3.1. Characterization of rGO/BSA/GA matrix structure

A key effort in this work was to form porous nanostructures on the surface of the microscale electrochemical sensors to accommodate increased number of target molecules compared with planar electrodes. However, a key challenge is that, patterning non-conductive nano-composites on the electrode surface can hinder electron transfer, thus decreasing electrical

current and detection sensitivity (Banerjee et al., 2011; Campuzano et al., 2019). To create the porous 3D nanostructure on planar electrodes while maintain the electroconductivity, therefore, we formed rGO/GA/BSA nanocomposite. Overall, in this construct, GA functions as an amine-reactive homo-bifunctional crosslinker to link BSA molecules and form the protein matrix (Habeeb and Hiramoto 1968; Kumar and Sundramoorthy 2019); meanwhile, rGO was used in the matrix as it is a commonly used functional material in biosensors due to its large surface area, excellent biocompatibility and electrical conductivity, (Taniselass et al., 2019; Zupančič et al., 2021) which is highly desirable for electrochemical characterizations. Besides, antifouling coating with GA-crosslinked BSA and rGO nanoflakes displayed exceptional porous 3D matrix structure for biomolecule characterization in biofluids (Timilsina et al. 2022, 2023; Zupančič et al., 2021).

More specifically, to immobilize the BSA/TEPA-rGO mixture on the surface of the electrochemical sensors, GA was used as crosslinker to react with the mixture, forming Schiff bases between the carbonyl ends of GA and the amine groups of BSA/TEPA-rGO. (Salem et al., 2010). The morphology of the rGO/BSA/GA matrix coating was characterized using SEM (Noran EDC Hitachi) (Fig. 2a). To ensure the successful surface modification of the sensor, the 3D nanocomposite-coated working electrode was characterized through Raman spectroscopy (Fig. S2). The Raman spectrum showed two typical peaks at 1350 cm^{-1} and 1580 cm^{-1}, which belonged to the G- and D-band of rGO respectively. The intensity ratio of G and D bands of rGO was 1.03, indicating a high density of structural defects (Luo et al., 2023). After the coating, a composite material was densely arranged onto the Au electrode surface, forming a roughened surface that can accommodate a larger number of target molecules (Fig. 2a i-ii, Fig. S3). To understand the changes in the electrical properties of the surface-modified electrodes, we characterized and compared the cyclic voltammograms of the electrochemical sensor before and after the matrix was coated on the electrode surface (Fig. 2b).

To optimize the sensitivity of the surface-modified electrochemical sensors, a key aspect was to optimize the concentration of rGO, the electrically conductive material in the nanocomposite. We tested varied concentration of rGO in BSA buffer (1 mg/mL, 2.5 mg/mL, 5 mg/mL and 10 mg/mL), and then characterized the correlation between the amount of rGO and the conductivity of the sensor. The conductivity was presented as the ratios of the CV current peak before and after coating in both oxidation and reduction stages. Results showed that the higher concentration of rGO led to higher electrical conductivity (Fig. S4 and Table S1). The rGO/BSA/GA coating sustained 78.89% (oxidation) and 69.44% (reduction) of current density at 10 mg/mL rGO condition. In addition, we evaluated voltammograms at various scan rates to examine the mass transport of potassium ferri-/ferrocyanide on rGO/BSA/GA-coated electrodes. The resulting cyclic voltammogram profiles were shown as in Fig. 2b and produced currents that were directly proportional to the square root of the scan rate, indicating a diffusion-limited process on the coated surface for electrochemical characterization.

3.2. Electrochemical response to the formation of immunoassay

To detect sPD-L1, an immunoassay was performed on the electrochemical sensor as depicted in Fig. 3a. First, the surface of the working electrode in the electrochemical sensor was coated with a 3D nano-composite of rGO/BSA/GA as detailed earlier; this step was to form a porous nanostructure, allowing for the migration of electroactive substrates to the proximity electrode, therefore improving overall electrochemical performance. The carboxyl groups in the rGO were then activated based on EDC/NHS chemistry so that they can be linked to antibodies in the subsequent step. Next, monoclonal anti-PD-L1 was added to the nanocomposite-modified working electrodes for incubation, and the remaining activated carboxyl groups were quenched using TBS and then blocked using superblock to minimize non-specific adsorption.

To ensure the success of each step during modification of the surface of the electrodes described above, electrochemical characterizations were then conducted on the electrode after each material and reagent was added. First, the DPV curves of rGO/BSA/GA (Fig. 3b) demonstrated a slight decrease compared with bare Au electrode, confirming the success of coating of the nanostructure. After the addition and incubation of the antibodies, the electrical current further decreased as anticipated; this can be explained by the poor electrical conductivity of these biomolecules which hindered the charge transfer between the surface of the sensors and the electrolyte solution. In fact, when varied concentrations of sPD-L1 (10 ng/mL, 1 μg/mL, and 10 μg/mL) were tested, there was a decrease in the DPV current signal with the increasing concentration, which was caused by the binding of antibodies to the target sPD-L1 molecules (Fig. 3b). A calibration curve was plotted for the DPV current signals, as shown in the inset of Fig. 3b, exhibiting excellent linearity with a correlation coefficient (R^2) value of 0.9645.

Meanwhile, EIS was performed as a second means to verify the changes in the impedance caused by the conjugation between the antibody and target protein. In EIS characterization, the impedance data was fitted using the Randle equivalent circuit, as shown in the inset of Fig. S5, which included the solution resistance (R_s), charge transfer resistance (R_{ct}), a constant phase element (CPE) representing the non-ideal behavior of the double layer capacitance, as well as a Warburg impedance element (Z_W). We conducted a comparison of the charge transfer resistance (Rct) of the electrochemical electrode at three concentrations. EIS characterization displayed a similar trend in R_{ct} (Fig. S5), which increased linearly with the concentration of sPD-L1($R^2 = 0.9978$).

Although the direct conjugation between the capture antibody and sPD-L1 demonstrated potential for the quantitative detection of sPD-L1 in the range of ng/mL to μg/mL using electrochemical sensing; this was a few magnitudes higher than commercial sPD-L1 ELISA kits with a linear range of 0.156–10 ng/mL (Aghajani et al., 2019). To enhance the electrochemical signal, we added the biotinylated detection antibody to form a sandwich immunoassay (Fig. 4a). After the conjugation between the detection antibodies and the target molecules, poly-HRP-streptavidin was then added to bind with the biotin molecules on the detection antibody. Precipitation TMB was then added to catalyze HRP, which can precipitate insoluble reaction product locally on the electrode where the enzyme was present (Timilsina et al., 2021). Although TMB + H_2O_2 enzymatic reaction with HRP is a common

strategy in electrochemical detection, in this work, we used the precipitation TMB instead as it can offer a mild acidic buffer that can minimize potential damage to the electrodes and nanocoating.

We further performed a quantitative detection of sPD-L1 in lower concentrations (1 pg/mL to 1 ng/mL) along with a negative control and a blank control as a validation. The negative control was performed by incubating sPD-L1 with a BSA-coated electrode, and the blank control was performed by incubating the anti-PD-L1-coated electrode surface with PBS. Results showed that a higher signal was obtained in the target samples than the controls, and the two controls presented no statistically significant difference on their signals (Fig. 4b). In the quantitative detection, DPV signals obtained from sPD-L1 in serial dilutions were presented in Fig. 4c. The current signals exhibited a good linear relationship with the logarithmic concentration of sPD-L1 in the range of 1 pg/mL to 1 ng/mL with R^2 of 0.9791 (Fig. 4d). The electrochemical sensor integrated in the DMF device displayed comparable performance compared with previously reported electrochemical methods (as summarized in Table S2).

We evaluated the selectivity of the sensor measuring human B7–H3 protein, a newly found molecule of B7 family expressed on the surface of tumor cells along with B7–H1 (PD-L1) (Yang et al., 2020). The current signal resulting from B7–H3 was significantly lower than that of sPD-L1 (Fig. S6), confirming desired selectivity. We also investigated the reproducibility of the sensors through repeated detection of sPD-L1 for five times, and the results showed a relative standard deviation of 6.69% among the measurements (Fig. S7). To further assess the stability of the sensors over time, the surface-modified sensors were stored at 4 °C and tested at varied intervals (Fig. S8). After being stored for 11 days, the sensors still retained 96.35% of initial electrochemical response to 1 ng/mL sPD-L1, indicating good stability.

3.3. Electrochemical detection of sPD-L1 secreted by human breast cancer cells

As a proof-of-concept demonstration of the functionality of the device and its potential use in biological and physiological fluids, we used this device to detect sPD-L1 molecules secreted by a human breast cancer cell line (MDA-MB-231) in the culture media. To validate our approach, we used MDA-MB-231 cell line transfected with a pcDNA3.1/PD-L1vector that contained full-length cDNA of human PD-L1 as our target sample, because these transfected cells had an overexpression of PD-L1 in the tumor cells that would secrete more sPD-L1. Meanwhile, we used the same cell line with PD-L1 knocked out by CRISPR/Cas9 technology as a negative control, because these cells were unable to express and secrete any PD-L1 in culture (Fig. 5a). We pipetted 20 uL of the media of each sample and directly loaded into our DMF device to perform the experiments.

The results in Fig. 5b illustrates the DPV signals obtained from the cell culture media: blank control as the baseline, the media in which the PD-L1 transfected human breast cancer cells (overexpressed PD-L1) were cultured, and the media in which the PD-L1 knocked-out human breast cancer cells were cultured. Overall, the target sample exhibited a notably higher DPV signal compared with the two controls, which confirmed that an amount of sPD-L1 were secreted by the pcDNA3.1/PD-L1 vector-transfected human breast cancer

cells. We observed ~2X increase in the magnitude of the obtained signal from the target sample compared with the control experiments (Fig. 5c). The outcome demonstrated the feasibility of detecting sPD-L1 from biofluids using the electrochemical sensors integrated into a DMF platform.

4. Conclusions

As new trends move toward the rapid detection of sPD-L1 in cancer immunotherapy, recent efforts have been directed toward the creation of sensitive electrochemical-based immunosensors and their integration with microfluidic technologies for POC testing. A key contribution of this work is the development of microscale electrochemical sensors modified with electrically conductive 3D matrix on their surface for the sensitive detection of sPD-L1 molecules and the integration of the microsensor array into a DMF platform to streamline and automate sample processing and target detection on-chip. The proof-of-concept platform can detect as low as 1 pg/mL sPD-L1 in 20 μL buffered samples and can also directly detect sPD-L1 secreted by human breast cancer cells in 20 μL culture medium. The sensors showed desired level of selectivity and stability over time. Our next step would focus on detecting sPD-L1 in microliters of human physiological fluids, such as plasma and eventually blood. A limitation of the platform is the complex microfabrication processes of the microsensor arrays that require multiple laborious steps in cleanroom, which poses challenge for the rapid and mass production of these devices. Our future efforts will be to integrate paper-based sensors into DMF platforms so that their unique advantages can be combined in a relatively easy manner. Ultimately, we envision that a platform as such can be translated into a POC tool to frequently monitor the level of sPD-L1 and other key indicators of the efficacy of cancer immunotherapy, which can eventually assist the physicians to make timely adjustment for each individual to maximize the benefit of cure.

Supplementary Material

Refer to Web version on PubMed Central for supplementary material.

Acknowledgement

This work was supported by the Ivan Bowen Family Foundation, the Department of Physiology and Biomedical Engineering and the Center for Individualized Medicine at Mayo Clinic (Rochester MN), and the National Institutes of Health (R35GM146651). The authors also thank the Division of Engineering at Mayo Clinic and Dr. Alexander Revzin for granting the access to their microfabrication facilities, as well as the Characterization Facility in College of Science & Engineering at the University of Minnesota – Twin Cities for their assistance with Raman spectroscopy.

Data availability

Data will be made available on request.

References

Aghajani MJ, Roberts TL, Yang T, McCafferty CE, Caixeiro NJ, DeSouza P, Niles N, 2019. Endocr Connect 8 (7), 1040–1051. [PubMed: 31252406]

Awad MM, Jones RE, Liu H, et al., 2016. Cancer Immunol. Res 4 (12), 1038–1048. [PubMed: 27856426]

Banerjee I, Pangule RC, Kane RS, 2011. Adv. Mater 23 (6), 690–718. [PubMed: 20886559]

Campuzano S, Pedrero M, Yáñez-Sedeño P, Pingarrón JM, 2019. Int. J. Mol. Sci

Chen Y, Wang Q, Shi B, Xu P, Hu Z, Bai L, Zhang X, 2011. Cytokine 56 (2), 231–238. [PubMed: 21733718]

Gong J, Chehrazi-Raffle A, Reddi S, Salgia R, 2018. J. Immun.Ther. Cancer 6 (1), 8.

Goto M, Chamoto K, Higuchi K, et al., 2019. Sci. Rep 9 (1), 10144. [PubMed: 31300681]

Habeeb AFSA, Hiramoto R, 1968. Arch. Biochem. Biophys 126 (1), 16–26. [PubMed: 4174905]

Han Y, Liu D, Li L, 2020. Am. J. Cancer Res 10 (3), 727–742. [PubMed: 32266087]

Herbst RS, Soria J-C, Kowanetz M,, et al.F.S., 2014. Nature 515 (7528), 563–567. [PubMed: 25428504]

Hu H, Cai G, Gao Z, Liang C, Yang F, Dou X, Jia C, Zhao J, Feng S, Li B, 2023. Analyst 148 (9), 1939–1947. [PubMed: 36916483]

Hu H, Ding Y, Gao Z, Li H, 2021. Sensor. Actuator. B Chem 331, 129442.

Kumar THV, Sundramoorthy AK, 2019. Anal. Chim. Acta 1074, 131–141. [PubMed: 31159933]

Li J, Lillehoj P.

Li J, Wang J, Grewal YS, Howard CB, Raftery LJ, Mahler S, Wang Y, Trau M, 2018. Anal. Chem 90 (17), 10377–10384. [PubMed: 30085658]

Li L, Gu Z, Zhou J-L, Yan B, Kong C, Wang H, Wang H-F, 2021. Chin. Chem. Lett 32 (11), 3416–3420.

Li X, Dai H-N, Wang Q, Imran M, Li D, Imran MA, 2020. Comput. Commun 160, 431–442. [PubMed: 32834198]

Li Y, Wang S, Zhao Y, Li Y, Wang P, Xie H, Zhao P, Li Y, Liu Q, Wei Q, 2023. Anal. Chem 95 (22), 8720–8727. [PubMed: 37224306]

Liu Y, Jeraldo P, Mendes-Soares H, Masters T, Asangba AE, Nelson H, Patel R, Chia N, Walther-Antonio M, 2021. ACS Omega 6 (39), 25642–25651. [PubMed: 34632220]

Liu Y, Papautsky I, 2019. Micromachines.

Luo Z, Yang D, Liu J, Zhao HY, Zhao T, Li BX, Yang WG, Yu ZZ, 2023. Adv. Funct. Mater 33 (15), 2212032.

Mahoney KM, Freeman GJ, McDermott DF, 2015. Clin. Therapeut 37 (4), 764–782.

Massari F, Santoni M, Ciccarese C, Santini D, Alfieri S, Martignoni G, Brunelli M, Piva F, Berardi R, Montironi R, Porta C, Cascinu S, Tortora G, 2015. Cancer treat. Rev 41 (2), 114–121. [PubMed: 25586601]

Merelli B, Massi D, Cattaneo L, Mandalà M, 2014. Crit. Rev. Oncol. Hematol 89 (1), 140–165. [PubMed: 24029602]

Moazzam P, Myekhlai M, Alinezhad A, Alshawawreh F.a.A., Bakthavathsalam P, Gonçales VR, Tilley RD, Gooding JJ, 2021. Chem. Commun 57 (20), 2559–2562.

Nelson WC, Kim C-JC, 2012. J. Adhes. Sci. Technol 26 (12–17), 1747–1771.

Nesline MK, Knight T, Colman S, Patel K, 2020. Clinical therapeutics, 42 (9), 1682–1698. e1687. [PubMed: 32747004]

Noguchi K, Shimomura T, Ohuchi Y, Ishiyama M, Shiga M, Mori T, Katayama Y, Ueno Y, 2020. Bioconjugate Chem. 31 (7), 1740–1744.

Ou Y-C, Webb JA, O'Brien CM, Pence IJ, Lin EC, Paul EP, Cole D, Ou S-H, Lapierre-Landry M, DeLapp RC, Lippmann ES, Mahadevan-Jansen A, Bardhan R, 2018. Nanoscale 10 (27), 13092–13105. [PubMed: 29961778]

Patsoukis N, Wang Q, Strauss L, Boussiotis VA Sci. Adv 6(38), eabd2712..

Sabaté del Río J, Henry OYF, Jolly P, Ingber DE, 2019. Nat. Nanotechnol 14 (12), 1143–1149. [PubMed: 31712665]

Salem M, Mauguen Y, Prangé T, 2010. Acta Crystallogr., Sect. F: Struct. Biol. Cryst. Commun 66 (Pt 3), 225–228.

Shien K, Papadimitrakopoulou VA, Wistuba II, 2016. Lung Cancer 99, 79–87. [PubMed: 27565919]

Sunshine J, Taube JM, 2015. Curr. Opin. Pharmacol 23, 32–38. [PubMed: 26047524]

Taniselass S, Arshad MKM, Gopinath SCB, 2019. Biosens. Bioelectron 130, 276–292. [PubMed: 30771717]

Timilsina SS, Durr N, Jolly P, Ingber DE, 2023. Biosens. Bioelectron 223, 115037. [PubMed: 36584477]

Timilsina SS, Durr N, Yafia M, Sallum H, Jolly P, Ingber DE, 2022. Adv. Healthcare Mater 11 (8), 2102244.

Timilsina SS, Jolly P, Durr N, Yafia M, Ingber DE, 2021. Acc. Chem. Res 54 (18), 3529–3539. [PubMed: 34478255]

Verma V, Sprave T, Haque W, Simone CB, Chang JY, Welsh JW, Thomas CR, 2018. J. Immun. cancer 6 (1), 1–15.

Wang T, Ran Y, He Y, Shi L, Zeng B, Zhao F, 2023. Biosens. Bioelectron 237, 115558. [PubMed: 37531891]

Xing Y, Liu J, Luo J, Ming T, Yang G, Sun S, Xu S, Li X, He E, Kong F, 2022. ACS Sens. 7 (2), 584–592. [PubMed: 35060694]

Xing Y, Liu J, Sun S, Ming T, Wang Y, Luo J, Xiao G, Li X, Xie J, Cai X, 2021. Bioelectrochemistry 140, 107789. [PubMed: 33677221]

Yang S, Wei W, Zhao Q, 2020. Int. J. Biol. Sci 16 (11), 1767. [PubMed: 32398947]

Zhang Y, Liu Y, 2022a. Sens. Diagnost 1 (4), 648–672.

Zhang Y, Liu Y, 2022b. Biosensors.

Zupančič U, Jolly P, Estrela P, Moschou D, Ingber DE, 2021. Adv. Funct. Mater 31 (16), 2010638.

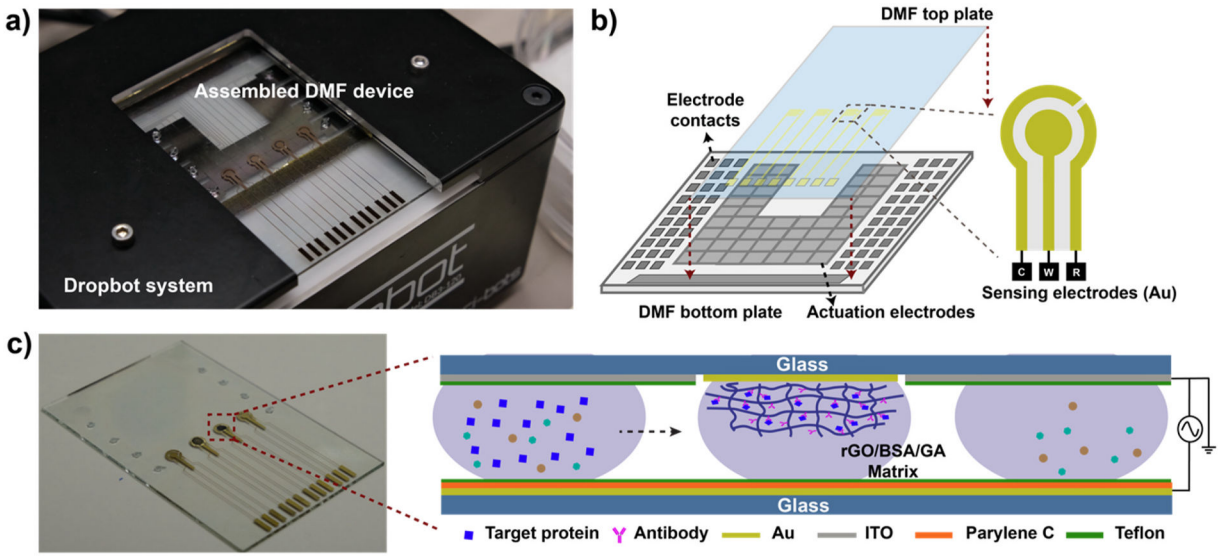

Fig. 1.

a) An assembled DMF device in a DropBot system; **b)** Overview of a DMF device with electrochemical sensors (not to scale). The bottom plate has 40 actuation electrodes for droplet handling. The top plate contains sensing electrodes that can be connected to an electrochemical workstation for signal detection. Each electrochemical sensor contains a working electrode (WE), a counter electrode (CE) and a reference electrode (RE); **c)** The sensing electrodes in the top plate are modified with 3D matrix structure. As a droplet moves across the electrode, target molecules are captured by the antibodies in the matrix.

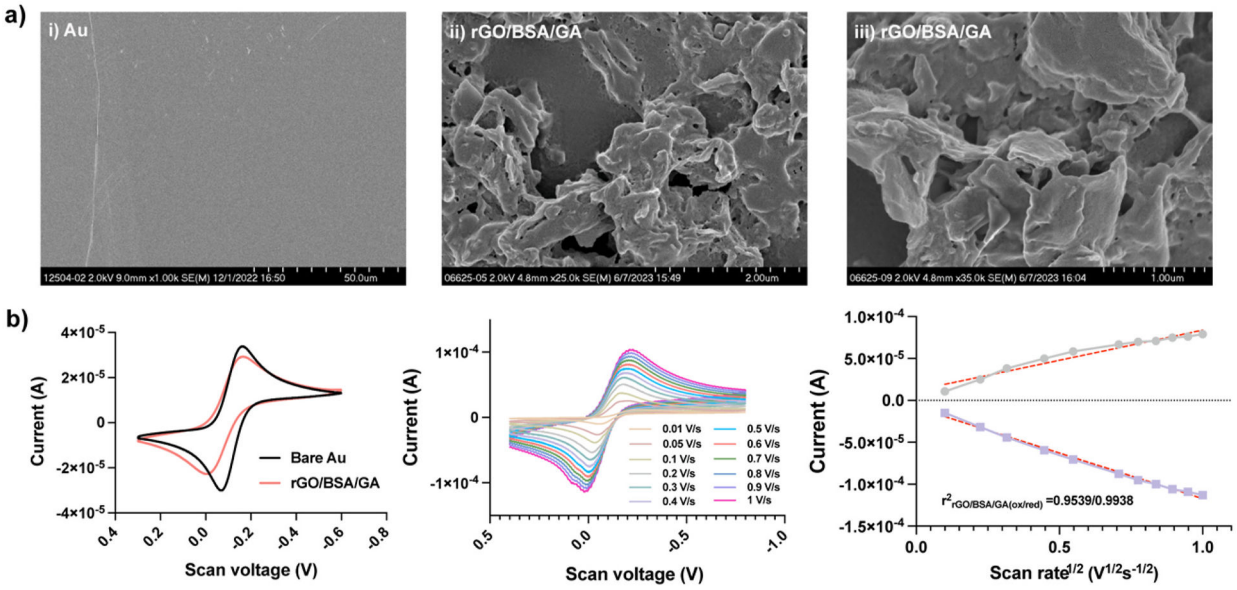

Fig. 2.

a) SEM images of the electrochemical electrode of **i)** bare Au electrode, and **ii)-iii)** after rGO/BSA/GA coating; **b) i)** Cyclic voltammogram (CV) characterization of electrochemical electrodes before (Bare Au) and after (rGO/BSA/GA matrix functionalization) in an equimolar solution of 10 mM K**3**[$Fe(CN)_6$]/K_4[$Fe(CN)_6$] and a supporting electrolyte of 0.1 M KCl; **ii)** CV representing oxidation and reduction of 5 mM ferri-/ferrocyanide solution using rGO/BSA/GA matrix coated Au electrode at different scan rates (0.01–1.0 V/s); **iii)** oxidation and reduction current rates of the ferri-/ferrocyanide couple against the square root of the scan rate.

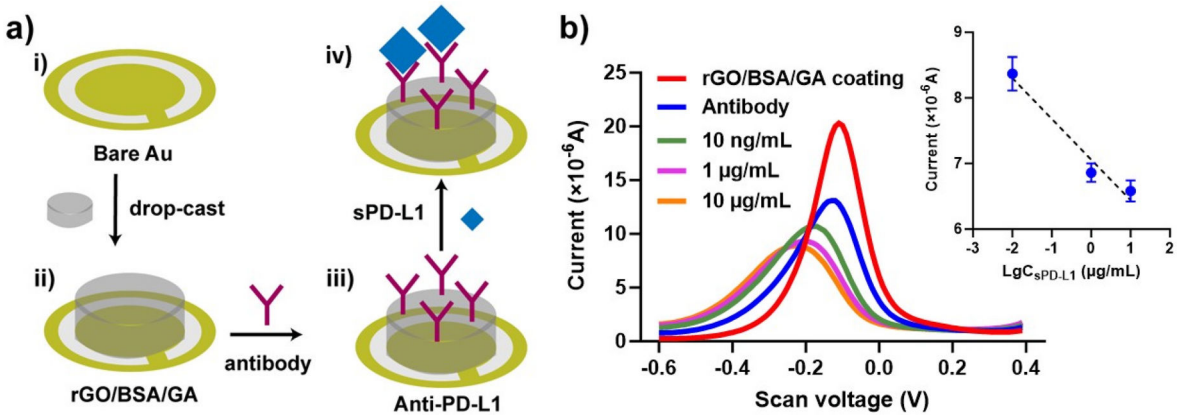

Fig. 3.

a) An illustration of a sandwich immunoassay on a biosensor coated with a porous 3D matrix structure. The process involves several steps: **i)- ii)** the electrochemical electrode was drop-casted with the rGO/BSA/GA nanocomposite; **iii)** the capture antibody was immobilized, followed by quenching and blocking using BSA; **iv)** PD-L1 sample was incubated, and the electrochemical characterization was performed to verify the binding; **b)** A differential pulse voltammogram (DPV) was obtained to measure the signal shifts at each step. The inset graph demonstrates the peak current caused by sPD-L1 conjugation at different concentrations. The error bar represents the standard deviation of n = 3.

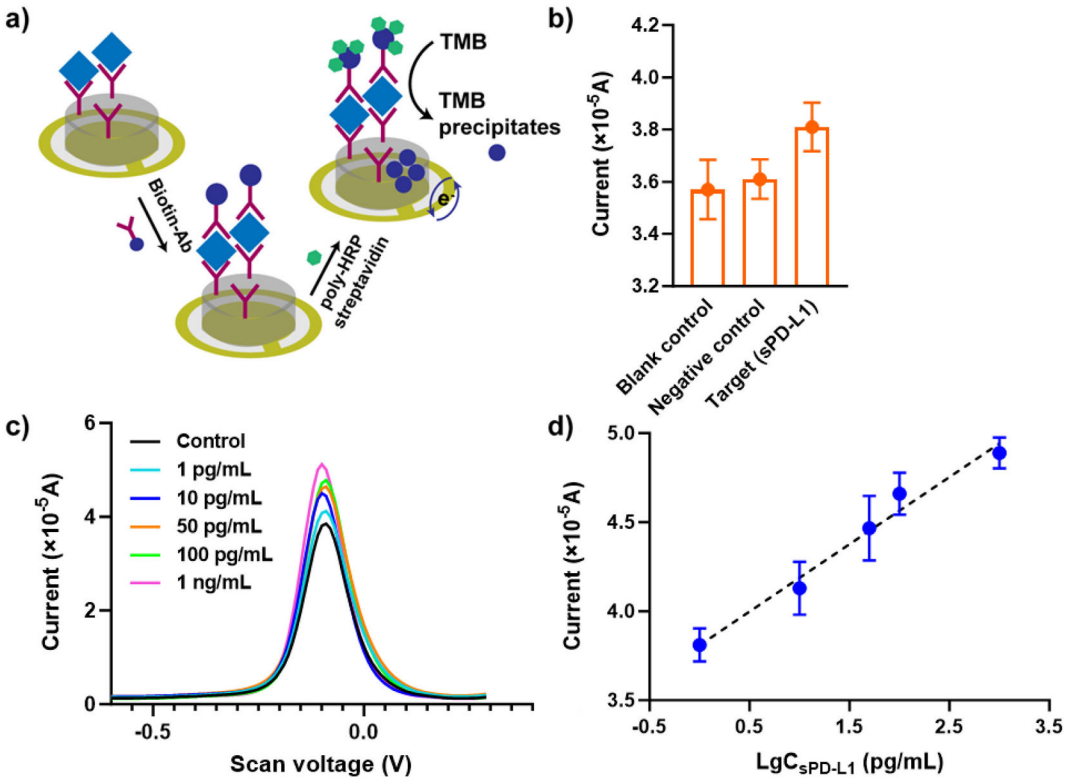

Fig. 4.

a) Captured PD-L1 was labeled with detection antibody conjugated with biotin, followed by conjugating with poly-HRP streptavidin. The electrochemical signal was measured by incubating the complex with precipitation TMB to catalyze the HRP. **b)** DPV signal comparison among blank control, negative control and target sPD-L1 sample (1 pg/mL). **c)** A quantitative detection of sPD-L1 at varied concentrations, and **d)** the relationship between the corresponding DPV signal magnitude and the logarithmic concentration of sPD-L1. The error bar represents the standard deviation of n = 4.

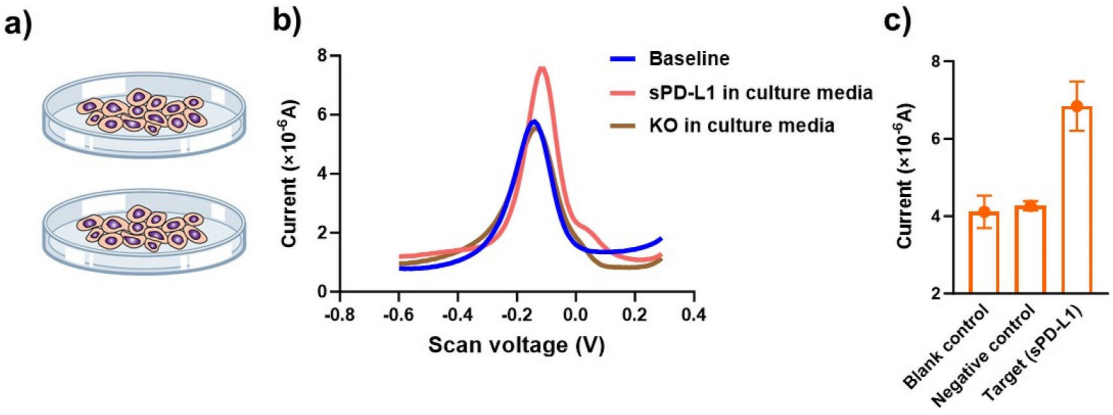

Fig. 5.

a) The culture of MDA-MB-231 cell line under two conditions i) transfected with pcDNA3.1 vector, which presented a higher level of sPD-L1 in cell culture media; ii) knock-out of PD-L1 using CRISPR/Cas9 technology, and presented absence of sPD-L1 in cell culture media; **b)** The DPV signals obtained from blank control (baseline); negative control (KO in culture media); and target (sPD-L1 in culture media), and the **c)** comparison of three samples plotted as bar graph. The error bar represents the standard deviation of n = 3.